

Analysis of Non-Coherent Joint-Transmission Cooperation in Heterogeneous Cellular Networks

Ralph Tanbourgi*, Sarabjot Singh[†], Jeffrey G. Andrews[†] and Friedrich K. Jondral*

Abstract—Base station (BS) cooperation is set to play a key role in managing interference in dense heterogeneous cellular networks (HCNs). Non-coherent joint transmission (JT) is particularly appealing due to its low complexity, smaller overhead, and ability for load balancing. However, a general analysis of this technique is difficult mostly due to the lack of tractable models. This paper addresses this gap and presents a tractable model for analyzing non-coherent JT in HCNs, while incorporating key system parameters such as user-centric BS clustering and channel-dependent cooperation activation. Assuming all BSs of each tier follow a stationary Poisson point process, the coverage probability for non-coherent JT is derived. Using the developed model, it is shown that for small cooperative clusters of small-cell BSs, non-coherent JT by small cells provides spectral efficiency gains without significantly increasing cell load. Further, when cooperation is aggressively triggered intra-cluster frequency reuse within small cells is favorable over intra-cluster coordinated scheduling.

Index Terms—Heterogeneous cellular networks, cooperation, non-coherent joint-transmission, stochastic geometry.

I. INTRODUCTION

The rapid increase of mobile traffic—primarily driven by data-intense applications such as video streaming and mobile web [1]—requires new wireless architectures and techniques. HCNs have attracted much interest due to their potential of improving system capacity and coverage with increasing density. Because of the opportunistic and dense deployment with sometimes limited site-planning, HCNs have at the same time contributed to rendering interference the performance-limiting factor [2]. Base station (BS) cooperation, which aims at increasing the signal-to-interference ratio (SIR) at victim users, is a promising technique to cope with newly emerging interference situations.

A. Related Work and Motivation

BS cooperation has been thoroughly analyzed in [3]–[8]. To address interference issues associated with heterogeneous deployments and to make use of the increased availability of wireless infrastructure, BS cooperation was also studied for HCNs. In [6] the authors demonstrated that with low-power BSs irregularly deployed inside macro-cell coverage areas, BS cooperation achieves higher throughput gains compared to the

macro-cell only setting, and hence as HCNs create new and complex cell borders more users profit from tackling other-cell interference through BS cooperation. The applicability of coordinated scheduling/beamforming (CS/CB) cooperation for HCNs was studied in [7], where it was found that practical issues such as accurate CSI feedback and tight BS synchronization required for coherent cooperation may disenchantingly limit the achievable gains. Such practical challenges associated with BS cooperation are by no means unique to HCNs [8], and hence other techniques with less stringent requirements have been studied as well. One such technique is non-coherent JT, in which a user’s signal is transmitted by multiple cooperating BSs without prior phase-mismatch correction and tight synchronization across BSs. At the user, the received signals are non-coherently combined, thereby providing opportunistic power gains. The standardization interest for non-coherent JT [9], [10], is particularly due to its *lower implementation complexity* for both the backhaul and the CSI feedback [11] and its ability for *balancing load* [7]; features of essential importance in HCNs [12].

Besides, analyzing BS cooperation in HCNs entails several challenges due to the many interacting complex system parameters, e.g., radio channel, network geometry, and interference. To make things even more difficult, these parameters typically differ across tiers, e.g., BS transmit power, channel fading or cell association. To address these challenges, *stochastic geometry* [13]–[15] has recently been proposed and used for analyzing cooperation in cellular networks [16]–[20].

B. Contributions

In this paper, we model and analyze non-coherent JT cooperation in HCNs. The contributions are summarized below.

Analytical model: A tractable model for HCNs with non-coherent JT is proposed in Section II. The model incorporates cooperation aspects of practical importance such as user-centric clustering and channel-dependent cooperation activation, each of which with a tier-specific threshold that models the complexity and overhead allowed in each tier. Other aspects such as BS transmit power, path loss, and arbitrary fading distribution are also assumed tier-specific.

Coverage probability: As the main result, the coverage probability under non-coherent JT is characterized in Section III for a typical user. The main result has a compact semi-closed form (derivatives of elementary functions) and applies to general fading distributions. We also propose a simple but accurate linear approximation of the coverage probability.

*The authors are with the Communications Engineering Lab, Karlsruhe Institute of Technology, Germany. Email: ralph.tanbourgi@kit.edu, friedrich.jondral@kit.edu. This work was supported by the German Research Foundation (DFG) within Priority Program 1397 “COIN” under grant No. JO258/21-1.

[†]The authors are with the Wireless and Networking Communications Group (WNCG), The University of Texas at Austin, TX, USA. Email: sarabjot@utexas.edu, jandrews@ece.utexas.edu

Design insights: *Load balancing:* Balancing load in two-tier HCNs, by additionally pushing more users to small cells in order to let these cells assist macro BSs with non-coherent JT, is favorable only to a limited extent. As small-cell cooperative clusters are increased, spectral efficiency gains grow only approximately logarithmically while cell load in those cells increases much faster. At small cluster sizes of small cells, generously stimulating cooperation by channel-dependent cooperation activation yields considerable spectral efficiency gains without consuming much radio resources.

Intra-cluster scheduling in small cells: When cooperation is aggressively triggered, small cells should reuse the resources utilized by non-coherent JT, i.e., intra-cluster frequency reuse (FR), to obtain cell-splitting gains. In lightly-loaded small cells with less aggressive triggering, not reusing these resources, i.e., intra-cluster CS, is better to avoid harmful interference.

II. MATHEMATICAL MODEL

A. Heterogeneous Network Model

We consider an OFDM-based co-channel K -tier HCN with single-antenna BSs in the downlink. The locations of the BSs in the k^{th} tier are modeled by a stationary planar Poisson point process (PPP) Φ_k with density λ_k . The BS point processes Φ_1, \dots, Φ_K are assumed independent. Every BS belonging to the k^{th} tier transmits with power ρ_k . A signal transmitted by a k^{th} tier BS undergoes a distance-dependent path loss $\|\cdot\|^{-\alpha_k}$, where $\alpha_k > 2$ is the path loss exponent of the k^{th} tier. Fig. 1 illustrates the considered scenario.

The entire set of BSs, denoted by Φ , is formed by superposition of the individual random sets Φ_k , i.e., $\Phi \triangleq \bigcup_{k=1}^K \Phi_k$. By [13], the point process Φ is again a stationary PPP with density $\lambda = \sum_k \lambda_k$. We assume single-antenna users/receivers to be distributed according to a PPP. By Slivnyak's Theorem [13], we evaluate the system performance at a *typical* receiver located at the origin without loss of generality.

The transmitted signals are subject to (frequency-flat) block-fading. The (power) fading gain from the i -th BS in the k^{th} tier to the typical user at the origin is denoted by g_{ik} . We assume that the g_{1k}, g_{2k}, \dots are i.i.d., i.e., the fading statistics may possibly differ across the K tiers. When appropriate, we will drop the index i in g_{ik} . We further require that $\mathbb{E}[g_{ik}] = 1$ and $\mathbb{E}[g_{ik}^2] < \infty$ for all i, k . Heterogeneous propagation conditions might, for instance, be due to different antenna heights across tiers. Thermal noise is neglected for analytical tractability but can be included in the analysis [19].

B. Non-Coherent Cooperation Model

BS clustering model: We employ a dynamic user-centric BS clustering method. In this method, BSs with sufficiently high average received signal strength (RSS) monitored at a given user form a cooperative cluster to cooperatively serve this user.¹ Transferring this to the model, the i -th BS from the k^{th} tier at location x_{ik} belongs to the cooperative cluster

¹Practical constraints typically impose additional criteria to this simple clustering rule for the associated overhead not to be overwhelming, cf. [8] for an elaborate discussion. We leave such possible extensions for future work.

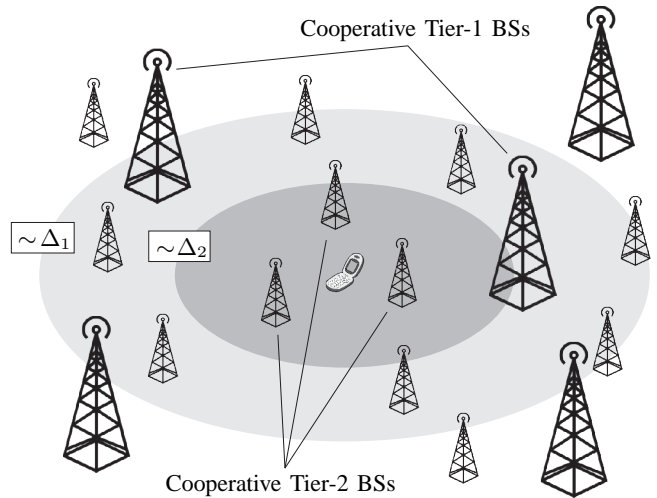


Fig. 1. Illustration of the considered scenario for the example of a two-tier cooperative HCN: Tier-1 BSs in range (inside lightly-shaded region with radius $\sim \Delta_1$) form a cooperative cluster for the typical user. Nearby Tier-2 BSs (inside dark-shaded region with radius $\sim \Delta_2$) join this cooperative cluster. All other nodes create out-of-cluster interference.

of the typical user if $\rho_k \|x_{ik}\|^{-\alpha_k} \geq \Delta_k$. Hereby, Δ_k denotes the k^{th} tier RSS threshold, which depends on the allowable cooperation overhead in the k^{th} tier and serves as a design parameter. The set of cooperative BSs from the k^{th} tier, then, has the form

$$\mathcal{C}_k \triangleq \left\{ x_{ik} \in \Phi_k \mid \|x_{ik}\| \leq \left(\frac{\Delta_k}{\rho_k} \right)^{-1/\alpha_k} \right\}. \quad (1)$$

The corresponding subset of non-cooperative BSs is denoted by $\bar{\mathcal{C}}_k \triangleq \Phi_k \setminus \mathcal{C}_k$.

Remark 1. *Practical user-centric clustering methods slightly differ from the above clustering model as the RSS difference to the serving BS is considered. Modeling this kind of clustering is analytically more involved and is deferred to future work.*

Channel-dependent cooperation activation: Whether a BS of a cooperative cluster gets engaged in a cooperative transmission to a particular user typically depends on its instantaneous channel to that user. To capture the basic impact of this channel-dependent mechanism, we use the following model: the i -th cooperative BS of the k^{th} tier joins a cooperative transmission to the typical user if $g_{ik} \rho_k \|x_{ik}\|^{-\alpha_k} \geq T_k$, where $x_{ik} \in \mathcal{C}_k$ and T_k is the cooperation activation threshold corresponding to the k^{th} tier. Similar to Δ_k , the variable T_k serves as a tunable design parameter to trade off performance against overhead. The subset of *active* cooperative BSs from the k^{th} tier serving the typical user is denoted as

$$\mathcal{C}_{a,k} \triangleq \left\{ x_{ik} \in \mathcal{C}_k \mid \|x_{ik}\| \leq \left(\frac{T_k}{g_{ik} \rho_k} \right)^{-1/\alpha_k} \right\}. \quad (2)$$

We denote by $\mathcal{C}_{\bar{a},k} \triangleq \mathcal{C}_k \setminus \mathcal{C}_{a,k}$ the set of cooperative BSs from the k^{th} tier not participating in the cooperative transmission to the typical user. These BSs may remain silent (intra-cluster CS) or may serve other users (intra-cluster FR) on the resources used for the cooperative transmission.

$$\mathcal{L}_{P_k}(s) = \exp \left\{ -\lambda_k \pi \rho_k^{2/\alpha_k} \mathbb{E}_{\mathbf{g}_k} \left[\max \left\{ \Delta_k, \frac{T_k}{\mathbf{g}_k} \right\}^{-2/\alpha_k} \left(1 - e^{-s \mathbf{g}_k \max \{ \Delta_k, T_k / \mathbf{g}_k \}} \right) + (s \mathbf{g}_k)^{2/\alpha_k} \Gamma \left(1 - \frac{2}{\alpha_k}, s \mathbf{g}_k \max \{ \Delta_k, \frac{T_k}{\mathbf{g}_k} \} \right) \right] \right\} \quad (8)$$

Non-coherent joint-transmission: In non-coherent JT, BSs scheduled for cooperative transmission to a user transmit the same signal without prior phase-alignment and tight synchronization to that user. At the user, the multiple copies are received non-coherently. At the typical user, the SIR can then be expressed as [19]

$$\text{SIR} \triangleq \frac{P}{J_{C_a} + J_{\bar{C}}}, \quad (3)$$

where

- $P \triangleq \sum_k \sum_{x_{ik} \in C_{a,k}} \mathbf{g}_{ik} \rho_k \|x_{ik}\|^{-\alpha_k}$ is the received signal power,
- $J_{C_a} \triangleq \sum_k \sum_{x_{ik} \in C_{a,k}} \mathbf{g}_{ik} \rho_k \|x_{ik}\|^{-\alpha_k}$ is the intra-cluster interference,
- $J_{\bar{C}} \triangleq \sum_k \sum_{x_{ik} \in \bar{C}_k} \mathbf{g}_{ik} \rho_k \|x_{ik}\|^{-\alpha_k}$ is the out-of-cluster interference.

Note that J_{C_a} in the denominator of (3) is zero when intra-cluster CS is assumed instead of intra-cluster FR. Also, the random variables P , J_{C_a} and $J_{\bar{C}}$ are mutually independent.

III. COVERAGE PROBABILITY

In this section, the coverage probability is derived for the typical user under non-coherent JT. It is defined as

$$P_c \triangleq \mathbb{P}(\text{SIR} \geq \beta) \quad (4)$$

for some threshold $\beta > 0$. Note that the distributions of P , $J_{\bar{C}}$ and J_{C_a} do not exhibit a closed-form expression in general. To get a better handle on the SIR in (3), we therefore propose an approximation of the sum interference $J_{C_a} + J_{\bar{C}}$ prior to characterizing the SIR for the considered model.

Proposition 1 (Interference approximation). *The sum interference $J_{C_a} + J_{\bar{C}}$ in (3) can be approximated by a Gamma distributed random variable \tilde{J} having distribution $\mathbb{P}(\tilde{J} \leq z) = 1 - \gamma(\nu, z/\theta)/\Gamma(\nu)$, where*

$$\nu = \frac{4\pi \left(\sum_k \frac{\lambda_k \rho^{-1/\alpha_k}}{\alpha_k - 2} \mathbb{E} \left[\mathbf{g}_k \max \left\{ \Delta_k, \frac{T_k}{\mathbf{g}_k} \right\}^{1 - \frac{2}{\alpha_k}} \right] \right)^2}{2 \sum_k \frac{\lambda_k \rho^{-1/\alpha_k}}{\alpha_k - 1} \mathbb{E} \left[\mathbf{g}_k^2 \max \left\{ \Delta_k, \frac{T_k}{\mathbf{g}_k} \right\}^{2 - \frac{2}{\alpha_k}} \right]} \quad (5)$$

is the shape parameter and

$$\theta = \frac{\sum_k \frac{\lambda_k \rho^{-1/\alpha_k}}{\alpha_k - 1} \mathbb{E} \left[\mathbf{g}_k^2 \max \left\{ \Delta_k, \frac{T_k}{\mathbf{g}_k} \right\}^{2 - \frac{2}{\alpha_k}} \right]}{2 \sum_k \frac{\lambda_k \rho^{-1/\alpha_k}}{\alpha_k - 2} \mathbb{E} \left[\mathbf{g}_k \max \left\{ \Delta_k, \frac{T_k}{\mathbf{g}_k} \right\}^{1 - \frac{2}{\alpha_k}} \right]} \quad (6)$$

is the scale parameter.

Proof: Since Φ_k and $\{\mathbf{g}_{ik}\}_{i=0}^{\infty}$ are mutually independent across tiers and by the linearity property of the expectation, the proof follows by computing the mean and variance of $J_{C_a} + J_{\bar{C}}$ using Campbell's Theorem [13] and applying a second-order moment-matching, see [19, Appendix B] for details. ■

For intra-cluster CS in the k^{th} tier, one has to set $T_k = 0$ in (5) and (6). The Gamma approximation of the sum interference created by Poisson distributed interferers was also previously used in [14], [19], [21], where the accuracy was found satisfactorily high. It can be applied whenever the interference has finite mean and variance.

Theorem 1 (Coverage probability). *The coverage probability of the typical receiver in the described HCN setting can be bounded above and below as*

$$P_c \underset{\tilde{\nu} = \lceil \nu \rceil}{\overset{\tilde{\nu} = \lfloor \nu \rfloor}{\gtrless}} 1 - \sum_{m=0}^{\tilde{\nu}-1} \frac{(\theta\beta)^{-m}}{m!} \frac{\partial^m}{\partial s^m} \left[\prod_k \mathcal{L}_{P_k}(-s) \right]_{s = \frac{1}{\theta\beta}}, \quad (7)$$

where $\mathcal{L}_{P_k}(s)$ is given by (8) at the top of this page.

Proof: See Appendix. ■

The worst-case gap between the lower and upper bound is equal to the value of the last summand $m = \lceil \nu \rceil - 1$. For integer-valued ν , either the upper or the lower bound becomes exact. A simple approximation to P_c can be obtained using a linear combination of the bounds in (7) with weights chosen according to the relative distance of ν to $\lfloor \nu \rfloor$ and $\lceil \nu \rceil$.

Corollary 1 (Linear approximation of P_c). *The coverage probability P_c can be approximated as*

$$P_c \approx 1 - \sum_{m=0}^{\lfloor \nu \rfloor - 1} \frac{(\theta\beta)^{-m}}{m!} \frac{\partial^m}{\partial s^m} \left[\prod_k \mathcal{L}_{P_k}(-s) \right]_{s = \frac{1}{\theta\beta}} - (\nu - \lfloor \nu \rfloor) \frac{(\theta\beta)^{-\lceil \nu \rceil + 1}}{(\lceil \nu \rceil - 1)!} \frac{\partial^{\lceil \nu \rceil - 1}}{\partial s^{\lceil \nu \rceil - 1}} \left[\prod_k \mathcal{L}_{P_k}(-s) \right]_{s = \frac{1}{\theta\beta}}. \quad (9)$$

As will be demonstrated later, the approximation in (9) turns out to be reasonable accurate despite its simple form. It may furthermore be interesting to study the P_c conditioned upon a fixed number of cooperating BSs in every tier. We denote by $P_k|C_k$ the combined received signal power from the k^{th} tier conditional on C_k cooperative k^{th} -tier BSs.

Corollary 2 (Conditional Laplace transform of $P_k|C_k$). *Conditioned on the fact that C_k tier- k BSs belong to the cooperative set of the typical user, the conditional Laplace transform of $P_k|C_k$ is*

$$\mathcal{L}_{P_k|C_k}(s) = \left(1 + \frac{\Delta_k^{2/\alpha_k}}{\lambda_k \pi \rho_k^{2/\alpha_k}} \log \mathcal{L}_{P_k}(s) \right)^{C_k}. \quad (10)$$

Remark 2. *Computing the m -th derivative in (7) is quite involved since (8) and (10) are composite functions. Generally, the m -th derivative of composite functions can be efficiently obtained by Faà di Bruno's rule and Bell polynomials, given that the derivatives of the outer and inner function are known.*

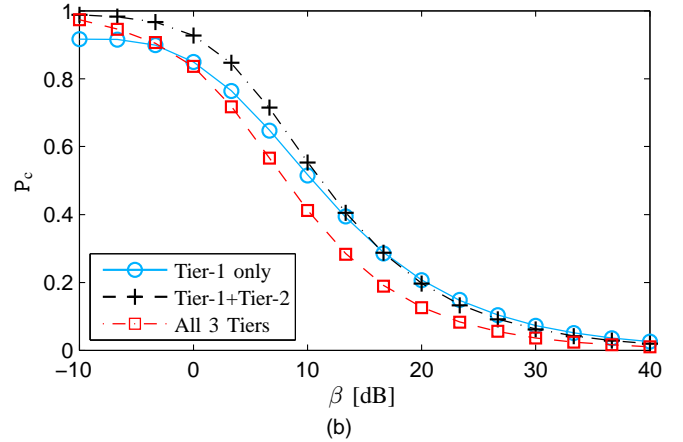
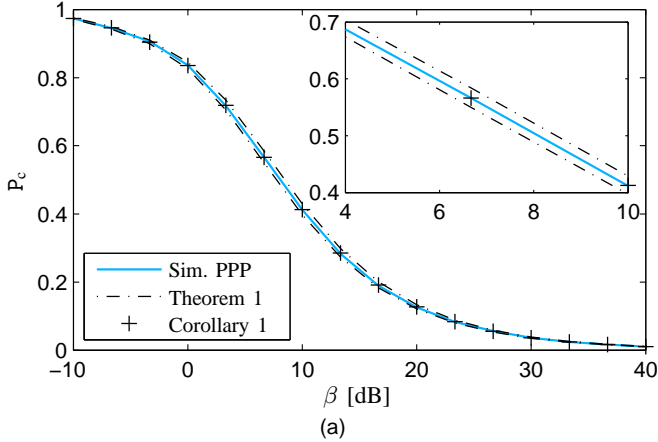


Fig. 2. Coverage probability P_c vs. SIR-threshold β . Simulation with Poisson interference (solid). Upper/lower bound from Theorem 1 (dash-dotted). Linear P_c -approximation from Corollary 1 (“+”-marks). The tier-specific parameters are shown in Table I.

We next derive the m -th derivative of the inner function (i.e., the exponent) of \mathcal{L}_{P_k} . The conditional case $\mathcal{L}_{P_k|C_k}$ can be obtained analogously.

Lemma 1. For $m > 0$, the m -th derivative of the exponent of $\mathcal{L}_{P_k}(-s)$ evaluated at $s = -\frac{1}{\theta\beta}$ is given by

$$\frac{\partial^m}{\partial s^m} \log \mathcal{L}_{P_k}(-s) \Big|_{s=-\frac{1}{\theta\beta}} = \frac{2\pi}{\alpha_k} \lambda_k \rho_k^{2/\alpha_k} (\theta\beta)^{m-2/\alpha_k} \times \mathbb{E} \left[\mathbf{g}_k^{2/\alpha_k} \Gamma \left(m - \frac{2}{\alpha_k}, \frac{\mathbf{g}_k}{\theta\beta} \max\{\Delta_k, \frac{T_k}{\mathbf{g}_k}\} \right) \right]. \quad (11)$$

For the unconditioned case, in particular, the computation of the required derivatives for obtaining (7) can be further simplified by exploiting the exponential form of (8).

Corollary 3. The differentiation $\frac{\partial^m}{\partial s^m} [\prod_k \mathcal{L}_{P_k}(-s)]_{s=-1/\theta\beta}$ for the unconditioned case can be computed by noting that

$$\frac{\partial^m}{\partial s^m} \left[\prod_k \mathcal{L}_{P_k}(-s) \right]_{s=-\frac{1}{\theta\beta}} = \frac{\partial^m}{\partial s^m} \mathcal{L}_P(-s) \Big|_{s=-\frac{1}{\theta\beta}} \quad (12)$$

where the outer function of \mathcal{L}_P is e^x and the inner function has derivative

$$\frac{\partial^m}{\partial s^m} \log \mathcal{L}_P(-s) \Big|_{s=-\frac{1}{\theta\beta}} = 2\pi \sum_{k=1}^K \frac{\lambda_k \rho_k^{2/\alpha_k}}{\alpha_k} (\theta\beta)^{m-2/\alpha_k} \times \mathbb{E} \left[\mathbf{g}_k^{2/\alpha_k} \Gamma \left(m - \frac{2}{\alpha_k}, \frac{\mathbf{g}_k}{\theta\beta} \max\{\Delta_k, \frac{T_k}{\mathbf{g}_k}\} \right) \right], \quad (13)$$

where $m > 0$.

IV. DISCUSSIONS AND NUMERICAL EXAMPLES

We now discuss the results obtained in Section III, in particular the accuracy of the linear approximation from Corollary 1. Numerical examples and design questions are also treated here.

Validation and accuracy: Fig. 2a shows the P_c for a HCN with $K = 3$ for different SIR-thresholds β . The tier-specific parameters are summarized in Table I. The chosen clustering thresholds Δ_k correspond to an average number of cooperative BSs $\mathbb{E}[C_1] = 3$, $\mathbb{E}[C_2] = 4$ and $\mathbb{E}[C_3] = 2$ in the PPP

TABLE I
HCN PARAMETERS USED FOR NUMERICAL EXAMPLES

Parameter	Tier-1	Tier-2	Tier-3
BS density λ_k	4 BS/km ²	16 BS/km ²	40 BS/km ²
BS power ρ_k	46 dBm	30 dBm	24 dBm
Path loss α_k	4.3	3.8	3.5
Nakagami- m_k	1.8	2.3	2.7
Clus.-thres. Δ_k	-69.6 dBm	-63.1 dBm	-49.5 dBm
Sched.-thres. T_k	Δ_1	$\Delta_2 + 3$ dB	$\Delta_3 + 3$ dB

model. It can be seen that the Gamma approximation of the interference from Proposition 1 is accurate as the gap between the lower and upper bound enclosing the simulated P_c is fairly small. Also, the simple approximation from Corollary 1 performs remarkably well (here, the shape is $\nu = 8.5$).

Effect of adding more tiers: Fig. 2b shows the impact on P_c when adding additional tiers. Interestingly, indicating the performance of non-coherent JT in terms of the number of tiers is not straightforward. For instance, the P_c for Tier-1+Tier-2 HCNs can be higher than for the case of three tiers. This is because, in this example, the clustering threshold Δ_3 in Tier-3 was chosen relatively high, e.g., due to complexity and overhead constraints, resulting in a rather unfavorable ratio of interference and cooperation. Hence, adding more tiers exhibits a non-monotonic trend in terms of P_c .

Effect of load balancing: Non-coherent JT can be used also for load balancing, which is especially important in HCNs to avoid under-/over-utilization of the different tiers. Due to transmit power imbalance between the different tiers, this typically means to push users towards smaller cells, e.g., by biasing cell association [22]. Balancing load using non-coherent JT is done by varying Δ_k , T_k of the corresponding small cells. Importantly, imprudently stimulating more cooperation by lowering Δ_k and/or T_k increases the SIR, however, possibly at the cost of an overwhelming load increase in the participating small cells. Using the developed model, this effect is analyzed next for the example of a 2-tier HCN. Since describing cell

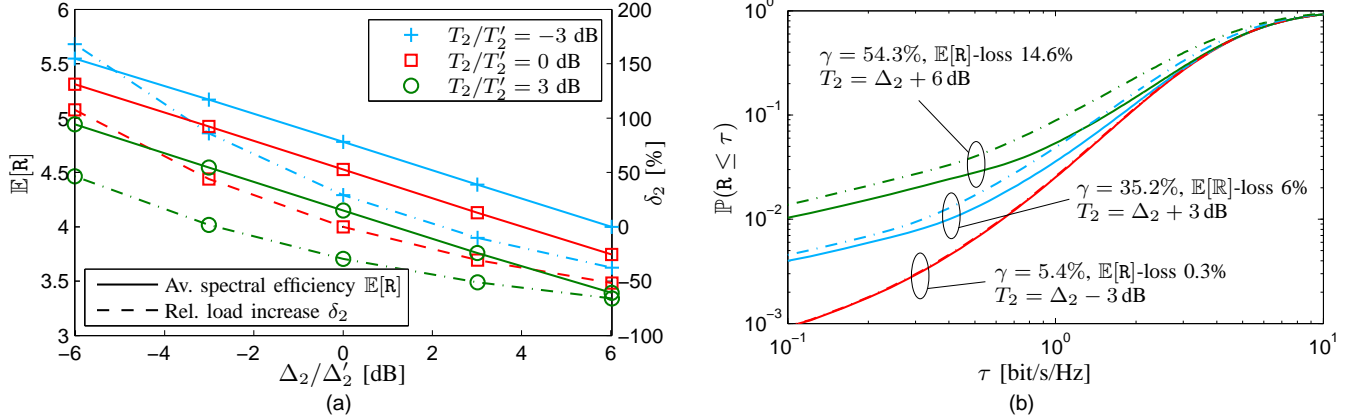


Fig. 3. Two-tier HCN: (a) Average R and relative load increase δ_2 for different Δ_2 , T_2 . (b) Distribution of R for intra-clustering CS (solid line) and FR (dashed line) for different T_2 . Also shown are the resource saving γ_2 in the small cells and the $\mathbb{E}[R]$ -loss when switching from CS to FR.

load in HCNs with cooperation is analytically difficult [19], we use a simple model for characterizing the load increase in the k^{th} -tier cell due to cooperation. Using (1) it can be seen that users closer than $(\Delta_k/\rho_k)^{-1/\alpha_k}$ to a k^{th} -tier BS request cooperation from that BS. Second, given the stationarity of the user point process, the number of radio resources N used for cooperation in a Tier-2 cell is proportional to the number of cooperation requests. Third, fixing an N' through some Δ'_k , T'_k , the load increase relative to N' measured as a function of Δ_k , T_k can then be defined as

$$\delta_k \triangleq \frac{\mathbb{E}[N(\Delta_k, T_k) - N(\Delta'_k, T'_k)]}{\mathbb{E}[N(\Delta'_k, T'_k)]}. \quad (14)$$

Applying Campbell's Theorem [13], [15] for evaluating the expectations in (14), we obtain

$$\delta_k = \frac{\mathbb{E}[\min\{\Delta_k, T_k/\mathbf{g}_k\}^{-2/\alpha_k}]}{\mathbb{E}[\min\{\Delta'_k, T'_k/\mathbf{g}_k\}^{-2/\alpha_k}]} - 1. \quad (15)$$

Remark 3. Note that (14) does not characterize the total cell load, but rather characterizes the underlying trend as a function of Δ_k and T_k , as these two parameters strongly influence the number of radio resources used for cooperation.

Fig. 3a shows how the average spectral efficiency $\mathbb{E}[R]$ and the relative load increase δ_2 in Tier-2 behave when varying Δ_2 , T_2 . The average spectral efficiency was obtained using the relation $R \triangleq \log_2(1 + \text{SIR})$ and $\mathbb{E}[R] = \int_0^\infty \text{P}_c(2^\beta - 1) d\beta$. It can be seen that $\mathbb{E}[R]$ increases approximately logarithmically (linearly) as Δ (in dB) decreases. At high Δ_2 , the load increase remains small, but rapidly accelerates as more clustering is stimulated through lowering Δ_2 . Interestingly, lowering the activation threshold T_2 does not change the load significantly at higher Δ_2 while providing considerable spectral efficiency gains. An important insight is that balancing load, by stimulating small cells (decreasing Δ_2 , T_2) to assist macro BSs through non-coherent JT, may be favorable only to a certain extent since the additional load imposed on small cells eventually outpaces the spectral efficiency gains.

Intra-cluster scheduling: An important design question in non-coherent JT is whether cooperating BSs not participating in an ongoing cooperative transmission 1) should reuse the radio resources allocated to non-coherent JT (intra-cluster FR) or 2) should remain silent on these resources to avoid intra-cluster interference, thereby virtually increasing cell load in these cells (intra-cluster CS). By trading off intra-cluster interference and cell load against cooperation, the impact of the two scheduling schemes is moreover intensified by the activation threshold T_k . In HCNs, in particular, intra-cluster FR might be favorable in small cells to obtain ‘‘cell-splitting’’ gains.

We next study whether intra-cluster FR or intra-cluster CS should be used in smaller cells using the following metric: switching from CS to FR invokes a resource saving at cooperative k^{th} -tier BSs not participating in non-coherent JT. This saving directly translates into a load reduction at those BSs, which we characterize as

$$\gamma_k \triangleq 1 - \mathbb{E}\left[\frac{\sum_{x_{ik} \in \mathcal{C}_k} \mathbb{1}(\mathbf{g}_{ik}\rho_k \|x_{ik}\|^{-\alpha_k} \geq T_k)}{\sum_{x_{ik} \in \mathcal{C}_k} \mathbb{1}(x_{ik} \in \mathcal{C}_k)}\right], \quad (16)$$

i.e., the *spatially*-averaged radio resource saving in cooperative k^{th} -tier cells of the typical user. The load reduction in (16) can be computed as

$$\gamma_k = 1 - \mathbb{E}\left[\min\left\{1, (\mathbf{g}_k \Delta_k / T_k)^{2/\alpha_k}\right\}\right]. \quad (17)$$

Interestingly, γ_k does not depend on λ_k and ρ_k . Fig. 3b shows the distribution of R for the example of a two-tier HCN for different T_2 . The value of Δ_2 was chosen such that $\mathbb{E}[C_2] = 5$. It can be seen that at low T_2 , switching from CS to FR does barely affect R (or $\mathbb{E}[R]$) while a load saving of approximately 5.4% is achieved. In this regime, FR may thus be more favorable. For larger T_2 one has to bite the bullet: much higher savings, e.g., 54.3%, can be obtained, however, at the cost of worsening R, e.g., $\mathbb{E}[R]$ -loss of 14.6%. In lightly-loaded cells CS should hence be used when a high T_2 is desired in order to additionally profit from muting intra-cluster interference.

V. CONCLUSION

We developed a tractable model and derived the coverage probability for non-coherent JT in HCNs, thereby accounting for the heterogeneity of various system parameters including BS clustering, channel-dependent cooperation activation, and radio propagation model. To the best of the authors' knowledge this is the first work to analyze cooperation in such generic HCNs. The developed theory allowed us to treat important design questions related to load balancing and intra-cluster scheduling.

APPENDIX

A. Proof of Theorem 1

We write

$$\begin{aligned} P_c &= \mathbb{E}_P [\mathbb{P}(J_{C_{\bar{a}}} + J_{\bar{c}} < P/\beta)] \\ &\stackrel{\text{Prop. 1}}{\approx} 1 - \mathbb{E}_P \left[\mathbb{P}(\tilde{J} \geq P/\beta) \right] \\ &= 1 - \mathbb{E}_P \left[\frac{\Gamma(\nu, P/\theta\beta)}{\Gamma(\nu)} \right]. \end{aligned} \quad (18)$$

Noting that $\Gamma(a, z)/\Gamma(a)$ is monotone increasing in a for all $z \geq 0$, we obtain the inequality

$$\begin{aligned} P_c &\stackrel{\substack{\tilde{\nu}=\lfloor \nu \rfloor \\ \tilde{\nu}=\lceil \nu \rceil}}{\leq} 1 - \mathbb{E}_P \left[\frac{\Gamma(\tilde{\nu}, P/\theta\beta)}{\Gamma(\tilde{\nu})} \right] \\ &= 1 - \sum_{m=0}^{\tilde{\nu}-1} \frac{(\theta\beta)^{-m}}{m!} \mathbb{E}_P \left[P^m e^{-P/\theta\beta} \right] \\ &= 1 - \sum_{m=0}^{\tilde{\nu}-1} \frac{(\theta\beta)^{-m}}{m!} \left. \frac{\partial \mathcal{L}_P(-s)}{\partial s^m} \right|_{s=\frac{-1}{\theta\beta}}, \end{aligned} \quad (19)$$

where $\mathcal{L}_P(s)$ is the Laplace transform of the combined received signal power. Due to the independence property of the Φ_1, \dots, Φ_K , we can decompose $\mathcal{L}_P(s)$ into $\prod_k \mathcal{L}_{P_k}(s)$, where $\mathcal{L}_{P_k}(s)$ is the Laplace transform corresponding to the received power P_k from tier k BSs. It can be obtained as

$$\begin{aligned} \mathcal{L}_{P_k}(s) &= \mathbb{E} \left[\exp \left\{ -s \rho_k \sum_{x_{ik} \in \mathcal{C}_{a,k}} g_{ik} \|x_{ik}\|^{-\alpha_k} \right\} \right] \\ &\stackrel{(a)}{=} \mathbb{E}_{\Phi_k} \left[\prod_{x_{ik} \in \mathbb{R}^2} \mathbb{E}_{g_{ik}} \left[\exp \left\{ -s \rho_k g_{ik} \|x_{ik}\|^{-\alpha_k} \right. \right. \right. \\ &\quad \left. \left. \left. \times \mathbb{1}(g_{ik} \rho_k \|x_{ik}\|^{-\alpha_k} \geq T_k) \mathbb{1}(\rho_k \|x_{ik}\|^{-\alpha_k} \geq \Delta_k) \right\} \right] \right] \\ &\stackrel{(b)}{=} \exp \left\{ -\lambda_k \int_{\mathbb{R}^2} 1 - \mathbb{E}_{g_k} \left[\exp \left\{ -s \rho_k g_k \|x\|^{-\alpha_k} \right. \right. \right. \\ &\quad \left. \left. \left. \times \mathbb{1}(\rho_k \|x\|^{-\alpha_k} \geq \max\{\Delta_k, \frac{T_k}{g_k}\}) \right\} \right] dx \right\} \\ &\stackrel{(c)}{=} \exp \left\{ -\frac{2\pi}{\alpha_k} \lambda_k \rho_k^{2/\alpha_k} \right. \\ &\quad \left. \times \mathbb{E}_{g_k} \left[\int_{\max\{\Delta_k, \frac{T_k}{g_k}\}}^{\infty} t^{-1-2/\alpha_k} (1 - e^{-s g_k t}) dt \right] \right\}, \end{aligned} \quad (20)$$

where (a) follows from the i.i.d. property of the g_{ik} , (b) follows from the probability generating functional of a PPP [13], [15], and (c) follows from interchanging expectation and integration and from the substitution $t = \rho_k \|x\|^{-\alpha_k}$. Eq. (8) then follows after partial integration. ■

REFERENCES

- [1] Cisco, "Cisco visual networking index: Global mobile data traffic forecast update, 20122017," white paper, Tech. Rep., Feb. 2013.
- [2] A. Ghosh *et al.*, "Heterogeneous cellular networks: From theory to practice," *IEEE Commun. Mag.*, no. 6, pp. 54–64, Dec. 2013.
- [3] D. Gesbert *et al.*, "Multi-cell MIMO cooperative networks: A new look at interference," *IEEE J. Sel. Areas Commun.*, vol. 28, no. 9, pp. 1380–1408, Dec. 2010.
- [4] R. Irmer *et al.*, "Coordinated multipoint: Concepts, performance, and field trial results," *IEEE Commun. Mag.*, vol. 49, no. 2, pp. 102–111, Feb. 2011.
- [5] A. Lozano, R. W. Heath Jr., and J. G. Andrews, "Fundamental limits of cooperation," *IEEE Trans. Inf. Theory*, vol. 59, no. 9, pp. 5213–5226, Sep. 2013.
- [6] D. Lee *et al.*, "Coordinated multipoint transmission and reception in LTE-advanced: deployment scenarios and operational challenges," *IEEE Commun. Mag.*, vol. 50, no. 2, pp. 148–155, Feb. 2012.
- [7] A. Barbieri *et al.*, "Coordinated downlink multi-point communications in heterogeneous cellular networks," in *IEEE Information Theory and Applications Workshop (ITA)*, 2012, pp. 7–16.
- [8] P. Marsch and G. Fettweis, Eds., *Coordinated Multi-Point in Mobile Communications*. Cambridge University Press, 2011.
- [9] 3GPP, "Coordinated multi-point operation for LTE physical layer aspects," TR 36.819, Tech. Rep., Sep. 2011.
- [10] Ericsson, "Discussions on DL CoMP schemes," 3GPP TSG-RAN WG1#66 R1-113353, Tech. Rep., Oct. 2011.
- [11] J. Li *et al.*, "Performance evaluation of coordinated multi-point transmission schemes with predicted CSI," in *IEEE Intl. Symposium on Personal Indoor and Mobile Radio Commun. (PIMRC)*, 2012, pp. 1055–1060.
- [12] J. G. Andrews *et al.*, "An overview of load balancing in HetNets: Old myths and open problems," *submitted to IEEE Commun. Mag.*, vol. abs/1307.7779, 2013, available at <http://arxiv.org/abs/1307.7779>.
- [13] D. Stoyan, W. Kendall, and J. Mecke, *Stochastic Geometry and its Applications*, 2nd ed. Wiley, 1995.
- [14] M. Haenggi and R. K. Ganti, "Interference in large wireless networks," *Found. Trends Netw.*, vol. 3, pp. 127–248, Feb. 2009.
- [15] M. Haenggi, *Stochastic Geometry for Wireless Networks*. Cambridge University Publishers, 2012.
- [16] K. Huang and J. Andrews, "A stochastic-geometry approach to coverage in cellular networks with multi-cell cooperation," in *IEEE Global Telecommunications Conference (GlobeCom)*, 2011, pp. 1–5.
- [17] H. P. Keeler, B. Błaszczyszyn, and M. K. Karray, "SINR-based coverage probability in cellular networks under multiple connections," in *IEEE Intl. Symposium on Inf. Theory (ISIT)*, 2013.
- [18] A. Giovanidis and F. Baccelli, "A stochastic geometry framework for analyzing pairwise-cooperative cellular networks," *ArXiv e-prints*, May 2013, available at <http://arxiv.org/abs/1305.6254>.
- [19] R. Tanbourgi, S. Singh, J. G. Andrews, and F. K. Jondral, "A tractable model for non-coherent joint-transmission base station cooperation," *ArXiv e-prints*, Jul. 2013, submitted to *IEEE Trans. Wireless Commun.*, available at <http://arxiv.org/abs/1308.0041>.
- [20] G. Nigam, P. Minero, and M. Haenggi, "Coordinated multipoint in heterogeneous networks: A stochastic geometry approach," in *Workshop on Emerging Technologies for LTE-Advanced and Beyond 4G, IEEE GlobeCom*, 2013, available at: www.nd.edu/~mhaenggi/pubs/globecom13b.pdf.
- [21] R. W. Heath Jr., M. Kountouris, and T. Bai, "Modeling heterogeneous interference using poisson point processes," *IEEE Trans. Signal Process.*, vol. 61, no. 16, pp. 4114–4126, Aug. 2013.
- [22] S. Singh, H. S. Dhillon, and J. G. Andrews, "Offloading in heterogeneous networks: Modeling, analysis, and design insights," *IEEE Trans. Wireless Commun.*, vol. 12, no. 5, pp. 2484–2497, Dec. 2013.